APL Photonics

Integrated amorphous silicon-aluminum long-range surface plasmon polariton (LR-SPP) waveguides

Cite as: APL Photonics 3, 036103 (2018); https://doi.org/10.1063/1.5013662
Submitted: 14 November 2017 . Accepted: 01 March 2018 . Published Online: 22 March 2018

Boaz Sturlesi, Meir Grajower, Noa Mazurski, and Uriel Levy

APL PHOTONICS **3**, 036103 (2018)

Integrated amorphous silicon-aluminum long-range surface plasmon polariton (LR-SPP) waveguides

Boaz Sturlesi, Meir Grajower, Noa Mazurski, and Uriel Levy
Department of Applied Physics, The Benin School of Engineering and Computer Science, The Center for Nanoscience and Nanotechnology, The Hebrew University of Jerusalem, Jerusalem 91904, Israel

(Received 14 November 2017; accepted 1 March 2018; published online 22 March 2018)

We demonstrate the design, fabrication, and experimental characterization of a long range surface plasmon polariton waveguide that is compatible with complementary metal-oxide semiconductor backend technology. The structure consists of a thin aluminum strip embedded in amorphous silicon. This configuration offers a symmetric environment in which surface plasmon polariton modes undergo minimal loss. Furthermore, the plasmonic mode profile matches the modes of the dielectric (amorphous silicon) waveguide, thus allowing efficient coupling between silicon photonics and plasmonic platforms. The propagation length of the plasmonic waveguide was measured to be about 27 μm at the telecom wavelength around 1550 nm, in good agreement with numerical simulations. As such, the waveguide features both tight mode confinement and decent propagation length. On top of its photonic properties, placing a metal within the structure may also allow for additional functionalities such as photo-detection, thermo-optic tuning, and electro-optic control to be implemented. https://doi.org/10.1063/1.5013662

I. INTRODUCTION

Over the last couple of decades, plasmonic devices attract growing attention due to their unique features such as tight light confinement, nanoscale light manipulation, and enhanced light-matter interactions. In the context of plasmonic waveguides, the presence of a metal within the structure may facilitate the possibility of co-propagation of overlapping electric and photonic signals and thus is of great interest. These unique characteristics can be utilized to allow diverse functionalities. And in fact, passive and active plasmonic devices provide ways to generate, guide,[1,2] modulate,[3–5] and detect[6–12] light with shrinking dimensions toward the scale of electronic devices. However, a major obstacle that one encounters when trying to realize plasmonic devices is the limited propagation length of the optical signal within a plasmonic waveguide, which is a direct result of light absorption (joule heating) in the metal. In an attempt to tackle this problem, various plasmonic waveguide configurations were proposed and demonstrated over the last few years. These include, for example, metallic strip,[13–15] gap,[16,17] nanowires,[18,19] V-groove,[20–24] long range surface plasmon polariton (LR-SPP) waveguides,[24,25] and dielectric loaded long range surface plasmon polariton (DL-LRSPP) waveguides.[26–29] Many of these waveguides offer longer propagation length of the signal at the expense of weaker spatial confinement and can be utilized for myriad applications.

So far, the vast majority of plasmonic waveguides were realized using low refractive index materials such as polymers as the dielectric environment. However, in order to integrate plasmonic technology with electronic circuitry on a chip, it is necessary for the materials used in the fabrication process to be compatible with the standard complementary metal-oxide semiconductor (CMOS) process. For this reason, silicon is a natural choice for the construction of plasmonic waveguides. Moreover, the use of a material with a high refractive index, such as silicon, enables further spatial confinement of the plasmonic mode and makes the waveguide cross section even more compact. In recent years, different silicon based plasmonic waveguides were suggested and analyzed theoretically[30–35] and even experimentally,[33] and novel configurations were suggested to reduce propagation loss.[36–38] Yet, these demonstrations are all based on bulk crystalline silicon or poly-silicon on insulator (SOI), preventing the use of these configurations in chip scale photonic communication devices, which are to be placed on top of a "ready-made" CMOS circuitry. For the latter, amorphous silicon (a-silicon) which is deposited at relatively low temperatures should be used. This is in contrast to poly silicon which is deposited at higher temperatures of about 600 °C, thus not suitable for backend applications in which the allowed thermal budget is limited. Additionally, gold and silver, which are widely used in plasmonic devices due to their lower light absorption, in particular, at the telecom regime, are both incompatible with the CMOS fabrication process and thus cannot be used in a commercial fabrication process. Therefore, one needs to consider alternative materials, which are CMOS compatible. Naturally, aluminum is a promising candidate due to its relatively low loss and its compatibility with CMOS processes.

In this work, we tackle these limitations by demonstrating for the first time a Long Range Surface Plasmon Polariton (LR-SPP) plasmonic waveguide with aluminum embedded in amorphous silicon. First, the device was designed and studied using a numerical vectorial eigenmode solver. Next, it was fabricated using the standard microelectronic planar process, utilizing the advantages and flexibility of amorphous silicon. This fact makes our device a viable candidate for chip scale integration with various optoelectronic components and easy to use with both its photonics and potentially electrical functionalities. Following the design and fabrication of the device, it was characterized experimentally by conducting spectral transmission measurements at telecom wavelengths around 1550 nm to measure the propagation length of the signal. We have also performed near field scanning optical microscope (NSOM) measurements to determine the modal content of the device and the effective refractive index of the modes.

II. DESIGN AND SIMULATIONS

The proposed long range surface plasmon polariton (LR-SPP) waveguide consists of a thin aluminum strip embedded inside amorphous silicon bulk which is placed on the deposited SiO_2 silicon wafer (Fig. 1). This configuration offers a symmetric environment in which the propagation loss of the SPP mode is minimized. The structure is designed to be compatible with CMOS technology, and for this reason, aluminum was our metal of choice. By using such a design, one can achieve both relatively long propagation length of the signal and wavelength scale mode confinement.

Using the Finite Difference Eigenmode solver (FDE, Lumerical Ltd.),[39] the mode profiles as well as their effective index and propagation loss at the telecom wavelength regime were calculated.

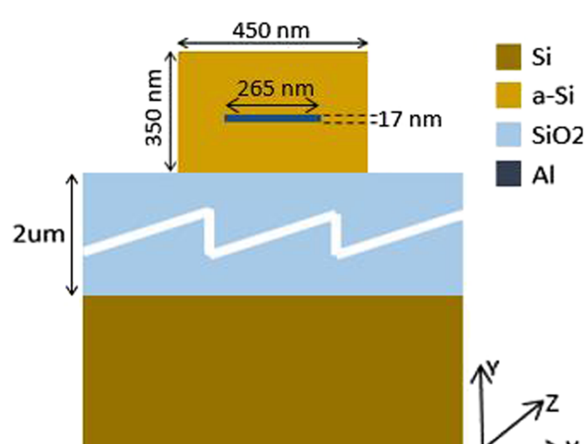

FIG. 1. Schematic cross section of the LR-SPP waveguide as designed with a thin aluminum strip (thickness t) embedded inside amorphous silicon bulk (thickness t and height h) deposited on a 2 μm SiO_2 substrate on a silicon wafer.

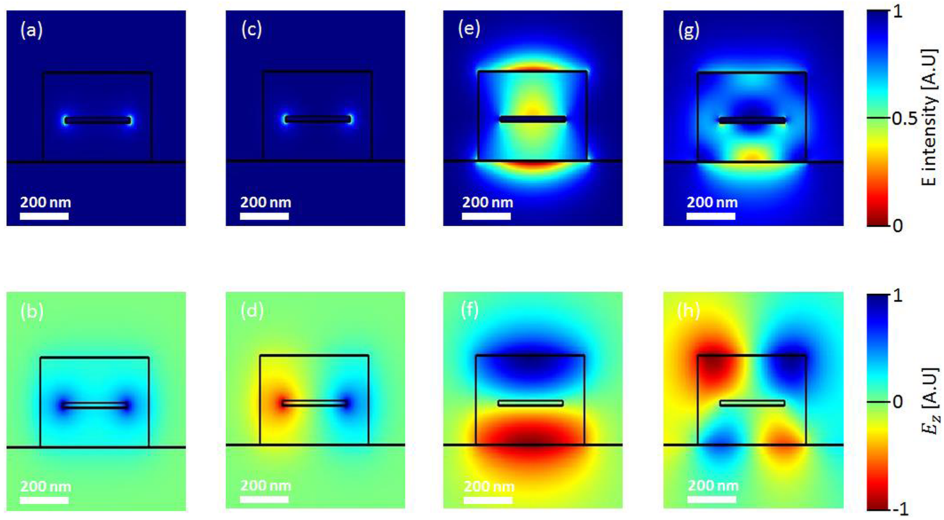

FIG. 2. Schematic cross section of the electric field intensity (top panel) and the longitudinal electric field component (bottom panel) of the modes sported by our waveguide at the wavelength of 1550 nm. [(a) and (b)] Fundamental SR mode with an effective index of 4.21 + 0.226i. [(c) and (d)] Second SR mode effective index of 3.807 + 0.259i. [(e) and (f)] Fundamental LR mode [(e) and (f)] with an effective index of 2.57 + 0.0036i. [(g) and (h)] Second LR mode [(g) and (h)] with an effective index of 1.695 + 0.013i.

The refractive index of SiO_2, a-Si, and Al was taken to be 1.55 + 0.18i, 3.471, and 1.44 + 16i in respect. Figure 2 presents the calculated electric field distribution of several modes supported by our waveguide. By examining the electrical field component along the propagation direction (Ez), one typically distinguishes between two types of modes: symmetric modes, where the electric field (Ez) is symmetric with respect to both sides of the metallic layer [Figs. 2(b) and 2(d)], and anti-symmetric modes, where the electric field (Ez) is antisymmetric with respect to both sides of the metallic layer [Figs. 2(f) and 2(h)]. These two types of modes differ drastically in their propagation loss and mode confinement. The two symmetric modes which are characterized by very large propagation loss of 7.972 dB/μm and 9.131 dB/μm, respectively, and tight mode confinement are referred to as Short-Range (SR) modes. Their effective refractive indices are 4.21 + 0.226i and 3.807 + 0.259i, respectively. On the other hand, the anti-symmetric modes exhibit a reduced propagation loss of 0.126 dB/μm and 0.453 dB/μm, respectively, together with a weaker mode confinement and referred to as Long-Range (LR) modes. Their effective refractive indices are 2.57 + 0.0036i and 1.695 + 0.013i, respectively. These features depend strongly on different parameters of the waveguide including the thickness of the metallic strip, its misalignment with respect to the a-silicon strip and the dimensions of a-Si. To optimize the waveguide design, we have performed numerical simulations to calculate the predicted attenuation and modal profiles as a function of the dimensions of the structure.

The propagation length depends strongly on the metal strip thickness. As shown in Fig. 3(a), examining the fundamental LR mode, the propagation length decreases dramatically as the metal strip becomes thicker, while for thin metal we can achieve very high propagation length. As an example, a 10 nm thick metal allows to achieve propagation length as high as 90 μm, while for 50 nm thick metal the propagation length decreases to about 5 μm. It is important to note that the high propagation length comes at the expense of a weaker spatial confinement. Considering practical issues regarding the fabrication process of high quality thin aluminum, and the need to achieve decent confinement, the metal thickness of the fabricated sample (to be discussed in Sec. III) was set to be 17 nm.

In order to experience minimal absorption loss, one should attempt to create a symmetric dielectric environment with respect to the metal plane. In our structure, the symmetry is slightly perturbed due to the presence of the oxide on top of the silicon substrate. To maximize the propagation length, the portion of the mode field with respect to both sides of the metal strip should be balanced. Thus, one needs to slightly modify the position of the aluminum strip along the y (height) direction in the

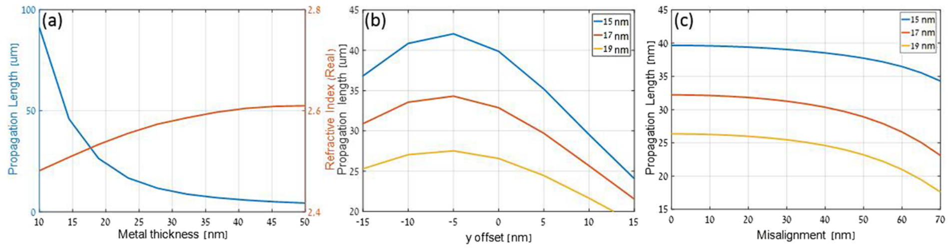

FIG. 3. (a) Effective propagation length and refractive index (real part) of the fundamental LR mode as a function of metal thickness. [(b) and (c)] Effective propagation length as a function of offset of the metal strip in the y (height) axis and horizontal misalignment from the center (x axis), respectively, for different metal thicknesses as that appear in the legend.

a-Si strip. As can be seen in Fig. 3(b), the maximal propagation length is obtained for a negative displacement of 5 nm from the center of the a-silicon strip.

In a realistic device implementation, one must also consider the possibility of misalignment between the aluminum and a-silicon strips. Such misalignment is the unavoidable result of the fabrication process. Figure 3(c) shows the dependence of the propagation length on the misalignment of the aluminum strip. It is noteworthy to mention that displacement of 50 nm results in a decay of only 10% in the propagation length. This indicates a high tolerance for misalignment due to the fabrication process.

The propagation length of the signal also depends on the geometrical properties of the waveguide. Figure 4 shows the propagation length of the fundamental mode as a function of the waveguide's height [Fig. 4(a)] and width [Fig. 4(b)] for a fixed metal width of 265 nm and several values of metal thickness as displayed in the legend. It can be seen that for larger dimensions of the waveguide we exhibit longer propagation lengths. These results are not surprising since larger dimensions of the waveguide cause the mode to be less confined to the metal stripe, hence exhibiting lower propagation loss.

According to our design, light is butt-coupled into the SPP waveguide from an a-Si waveguide with identical dimensions, except without the aluminum strip. As shown in Fig. 5, the a-Si waveguide supports 3 modes: a TE mode, a TM mode, and a hybrid mode. This is in contrast to our SPP waveguide which supports 4 modes, as previously showed in Fig. 2. In practice, the coupling efficiency to each of the SPP modes is greatly depending on the exciting photonic mode. The coupling efficiency between the plasmonic and photonic modes is estimated by calculating the vector overlap integral. It is evident that the photonic TM mode and the fundamental LR-SPP mode have a similar mode profile, which indicates an efficient coupling between them, as the overlap integral between them shows up to 98% coupling efficiency, with good tolerance to the offset of the metal strip. Furthermore, it is found that the hybrid photonic mode and the second LR-SPP mode exhibit up to 60% coupling efficiency, while the TE photonic mode couples very poorly to the plasmonic modes, as it shows only 20% coupling

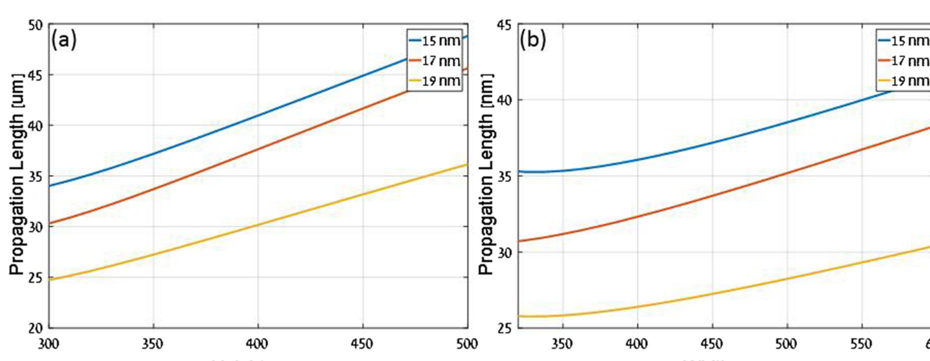

FIG. 4. Effective propagation length as a function of the waveguide's height for a fixed width of 450 nm (a) and waveguides width for a fixed height of 350 nm (b) for different thicknesses of the metal strip as that appear in the legend.

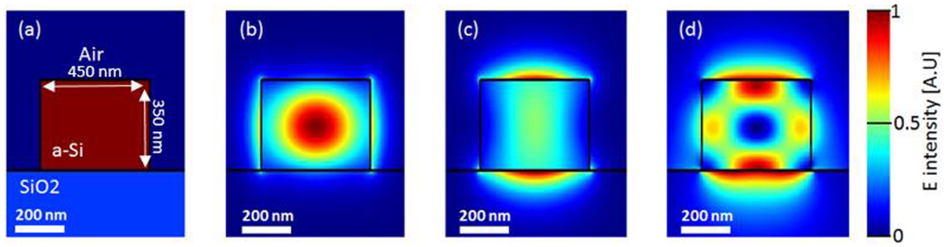

FIG. 5. (a) A schematic cross section of the a-Si waveguide which is used for coupling of light into the SPP waveguide. [(b)-(d)] The electric field intensity distributions of the modes sported by the a-Si waveguide: (b) TE mode (effective index of 2.466), (c) TM mode (effective index of 2.295), and (d) hybrid mode (effective index of 1.51).

efficiency to the second SR SPP mode and a negligible coupling to the fundamental LR-SPP mode. Based on these results, it is reasonable to expect that by launching a TM polarized light into our photonic waveguide, we will mostly excite the LR-SPP modes while the coupling to the SR SPP modes will be negligible.

III. FABRICATION

The fabrication process of the device is depicted in Fig. 6. A silicon wafer covered by a 2 μm thick thermal oxide is used as the raw material. First, a 170 nm thick layer of a-silicon is deposited using Plasma Enhanced Chemical Vapor Deposition (PECVD). Next, fine alignment marks are patterned using e-beam lithography and reactive ion etching (RIE). Then, the thin aluminum strip is defined using e-beam lithography followed by lift-off. To do so, a 17 nm thick aluminum layer is thermally evaporated on the patterned PMMA electron beam resist, and lift-off is performed in hot acetone. Next, an additional layer of 180 nm of a-silicon is deposited using PECVD. Finally, the waveguide and grating coupler boundaries are defined using e-beam lithography (using ZEP A520 as e-beam resist) followed by etching the full height of the amorphous silicon layer and reaching the oxide layer with RIE.

Figure 7 shows a top view scanning electron microscope (SEM) image of a typical device [Fig. 7(a)] and a cross section obtained using the focused ion beam (FIB) [Fig. 7(b)]. Grating couplers are used to couple light into and out of the a-silicon waveguides.

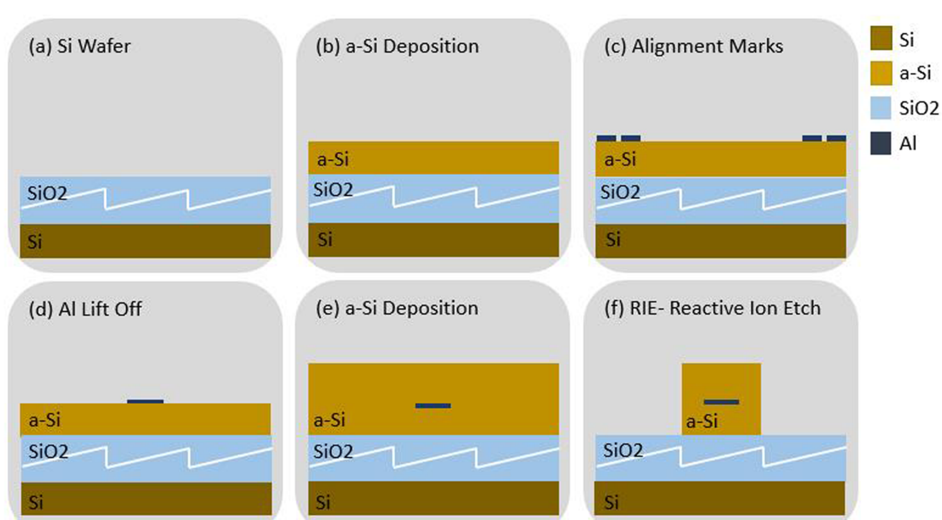

FIG. 6. Schematic description of the fabrication process flow: (a) planar substrate, (b) amorphous silicon deposition, (c) alignment marks, (d) aluminum lift-off, (e) amorphous silicon deposition, (f) reactive ion etching (RIE).

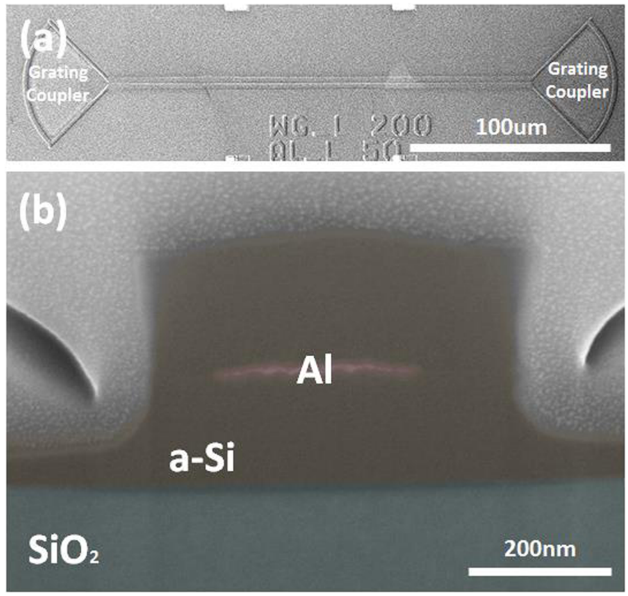

FIG. 7. (a) SEM image showing a top view of typical device grating couplers and waveguide trenches are visible. (b) Cross-sectional image of a typical device obtained using the focused ion beam (FIB). The different materials are highlighted in false colors. The bright material on the top is a protection layer used for the purpose of the FIB imaging process.

IV. EXPERIMENTAL RESULTS

To characterize the propagation length of the LR-SPP waveguide, we measured and analyzed the transmission of the optical signal through devices with different lengths of the aluminum strip. A diode laser is used to generate polarized light in the wavelength range of 1540-1560 nm. The signal was launched into a polarization maintaining cleaved optical fiber. For optimum coupling of light to the waveguide, we used grating couplers with 50 periods and a fill factor of 50%. To simplify the fabrication process, the gratings were fully etched into the a-silicon layer. The period of the gratings is ranging between 650 and 800 nm. The end facet of the optical fiber is precisely positioned above the grating coupler with a mechanical XYZ-translation stage. To achieve maximum coupling efficiency, the fiber is tilted from the normal at an angle of 10°. The coupled light propagates through the photonic waveguide and couples into the plasmonic waveguide and back into the photonic waveguide. Finally, light is coupled out of the device through another similar grating coupler, collected by another cleaved single mode fiber and detected by an InGaAs photodetector (HP 81634A).

As a reference, we have first measured the propagation loss of the a-Si waveguide without a plasmonic section. For this purpose, we have fabricated several such devices on a chip, consisting of a-Si waveguide and a grating coupler, varying in their length in the range of 100-400 μm, and measured the transmission through the different waveguides. To diminish the effect of Fabry-Perot oscillations, we performed each measurement by scanning the wavelength in the range of 1540-1560 nm and extracted the mean value of transmission. The results are presented in Fig. 8(a). By preforming a linear fit to the measured data, we found the propagation loss of the a-Si waveguide to be 12.8 ± 4.7 (dB/mm). The measured loss is larger than that reported in other studies[40] and is attributed to the quality of a-Si obtained after fabrication. Yet, due to the short length of the a-Si waveguide, this loss is negligible in comparison to the loss of the LR-SPP waveguide and thus can be ignored.

Next, we have used a similar method to measure the propagation loss of the plasmonic waveguide. This time we have fabricated several devices on a chip. Each device consists of a pair of grating couplers and a waveguide with a section containing aluminum strips with various lengths. The overall length of the device (i.e., the distance between the input and output grating coupler) was kept at a constant value of 200 μm, and the only variable parameter was the length of the aluminum strip. This configuration allows us to eliminate bias in the measurements which can originate, e.g.,

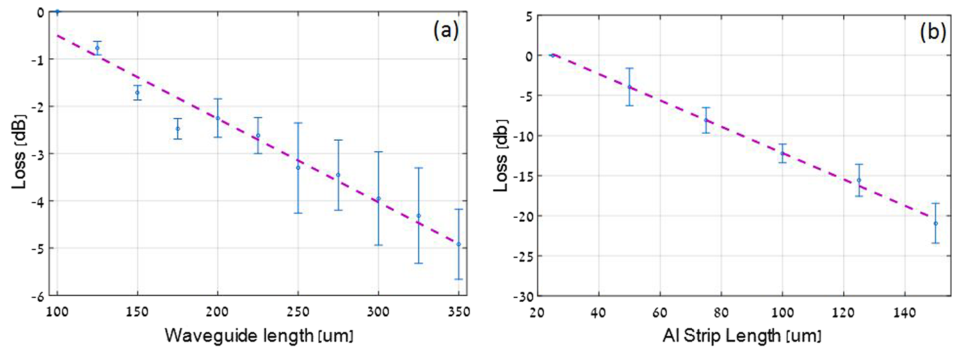

FIG. 8. Loss as a function of the a-Si waveguide length (a) and the LR-SPP waveguide length (b). In blue are measured values with the error bar showing the standard deviation; in magenta is a linear fit.

from surface reflection or direct scattering from the input fiber to the output fiber. We have performed transmission measurements for 7 different sets of devices, with an aluminum strip ranging between 25 μm and 150 μm. From these measurements, we could extract the propagation loss of the fundamental LR-SPP. Assuming that all other modes have vanished due to strong decay in the first few microns, the measured propagation loss is associated with the fundamental LR mode. The results of the mean transmission value are presented in Fig. 8(b), with the error bar showing the standard deviation of the seven measurements. By preforming a linear fit, we can easily extract the propagation loss, which was found to be 0.161 ± 0.015 (dB/μm), corresponding to a propagation length of 27.01 ± 2.8 μm. This result is in good agreement with the numerical simulations, predicting a loss of 0.126 (dB/μm) for the fundamental LR mode, (Fig. 4). The slightly shorter propagation length that was measured can be primarily explained by the roughness of the metal strip. Another reason can be related to the misalignment in the aluminum strip with respect to the waveguide, as indicated by the FIB cross section [Fig. 7(b)].

In order to further characterize the modes supported by our waveguide, we conducted Near-field Scanning Optical Microscopy (NSOM, Nanonics MultiView 4000) measurements using a metal coated probe with an aperture of 200 nm. Three sections of the waveguide were scanned—a section of photonic waveguide, a section of plasmonic waveguide, and a section containing the interface between the two. Each scan area was performed on an area of 25 × 25 μm (256 × 256 pixels). The measurement was carried out by scanning the top section of the waveguide, with light being coupled to the chip as in the previous case. Figure 9 shows the near field optical distribution measured in the three sections. The results reveal clear differences between the photonic and plasmonic sections of the waveguide. In the photonic section, the average field intensity remains constant along the propagation direction, whereas a significant decay appears in the plasmonic section. At the interface between the two sections, we observed back reflections and a clear transition from a non-attenuated to attenuated wave.

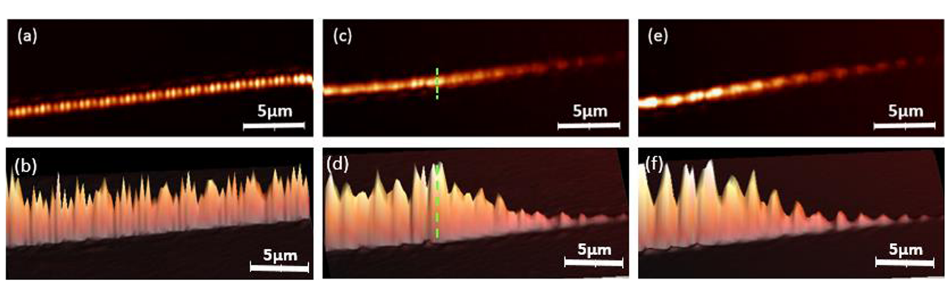

FIG. 9. Near field scanning optical microscope (NSOM) measurements: Top view (a) and 3D view (b) of field intensity in the photonic section of the waveguide. Top view (c) and 3D view (d) of the intersection between plasmonic and photonic sections of the waveguide; the change in trend is indicated with the green dashed line. Top view (e) and 3D view (f) of the plasmonic section of the waveguide.

Furthermore, a trace of modal beating effect is evident by the periodic intensity oscillations along the propagation direction for all measured sections. To better analyze the nature of these oscillations, we have performed a one dimensional Fourier transform to the measured data, from which we could determine the periodicity of the beating in each section. It was found that the photonic section contains two dominate spatial frequencies of 0.56 $\frac{1}{\mu\text{m}}$ and 1.89 $\frac{1}{\mu\text{m}}$, respectively. The lower frequency can be associated with a beating between the TM mode (having normalized propagation constant of 1.48 $\frac{1}{\mu\text{m}}$) and the hybrid mode (having normalized propagation constant of 0.97 $\frac{1}{\mu\text{m}}$), which are both supported by the photonic waveguide as calculated numerically [Figs. 5(c) and 5(d)]. The higher spatial frequency can be associated with a beating of the counter propagating signals carried by the hybrid mode. The counter propagation is the result of reflections from the interface.

The Fourier transform of the light propagating in the plasmonic section of the waveguide reveals a single dominant spatial periodicity of 0.58 $\frac{1}{\mu\text{m}}$. This may well indicate that both the first order and the second order LR modes coexist in the waveguide. As predicted by the numerical simulations, the spatial frequencies of these modes are 1.658 $\frac{1}{\mu\text{m}}$ [Fig. 2(e)] and 1.093 $\frac{1}{\mu\text{m}}$ [Fig. 2(g)], respectively. The existence of the two long range modes is reasonably expected. This is due to the fact that both the TM mode and the hybrid mode were evident in the photonic waveguide, and from mode overlap calculations, these modes are expected to couple with high efficiency to the first and second LR modes, respectively. The existence of the LR2 mode which suffers high propagation loss (0.58 dB/μm) explains the strong decay in the intensity, which is observed in the NSOM scan of the plasmonic section. Evidently, the strong decay can be mostly attributed to the high decay rate of this mode. As propagating along the waveguide, this mode is quickly vanishing and as a result the fundamental LR-SPP mode remains the dominant mode. Thus, the propagation loss of the signal is gradually associated with this mode.

V. DISCUSSION AND CONCLUSIONS

In this work, we have experimentally demonstrated for the first time a Long Range Surface Plasmon Polariton (LR-SPP) waveguide with aluminum embedded in a-silicon. To optimize the design of the device, we conducted numerical simulations and studied the effect of different parameters of the structure on the modal content, the absorption loss, and the effective index of the signal. We have found that a misalignment of few tens of nanometers is still tolerable from the point of view of propagation loss. Based on these simulations, we have set the geometry of the waveguide to achieve minimal absorption loss of the fundamental LR mode.

Following the device fabrication, it was characterized experimentally by conducting spectral transmission measurements at telecom wavelengths around 1550 nm. The propagation loss of the signal in the LR-SPP waveguide was measured to be 0.161 ± 0.015 (dB/μm), corresponding to a propagation length of 27.01 ± 2.8 μm. This measured propagation loss is associated with the fundamental LR mode. This result is in good agreement with the numerical simulations, predicting a loss of 0.126 (dB/μm). Further characterization of the device was conducted by preforming near field scanning optical microscope (NSOM) measurements. Using these measurements, we were able to determine the modal content and behavior of the signal in the device. The results reveal a strong decay in the average field intensity of the signal along the propagation direction in the plasmonic waveguide, whereas in the photonic waveguide the intensity remains constant. Furthermore, a trace of modal beating effect is evident, by which we can deduce the existence of two modes (a TM mode and a hybrid mode) in the photonic waveguide and subsequently two LR modes in the LR-SPP waveguide. These measurements correspond to the numerical simulations we conducted. Future waveguide design can be tailored to support a single LR-SPP mode by reducing the width of the waveguide to below 250 nm. With such a design, the second mode is above cutoff and cannot be supported.

The demonstrated structure is compatible with the CMOS process and is relatively easy to fabricate. The device features both tight mode confinement and decent propagation length. The use of amorphous silicon allows great flexibility and high compatibility to different integrated devices. Furthermore, the metal which is embedded within the structure may allow for multiple functionalities such as photo-detection, thermo-optic tuning, and electro-optic control to be achieved, which can be useful in a variety of applications. As been shown in recent studies,[3,5] plasmonic modulation of a signal in the telecom wavelength around 1550 nm can be achieved in a length of 30 μm and below. The suggested configuration may provide a base for the realization of such a device.

SUPPLEMENTARY MATERIAL

See supplementary material for the complete study and analysis of the grating couplers used for light coupling to the device.

[1] P. Berini, R. Charbonneau, N. Lahoud, and G. Mattiussi, J. Appl. Phys. **98**, 043109 (2005).
[2] R. Charbonneau, N. Lahoud, G. Mattiussi, and P. Berini, Opt. Express **13**, 977 (2005).
[3] A. Melikyan, L. Alloatti, A. Muslija, D. Hillerkuss, P. C. Schindler, J. Li, R. Palmer, D. Korn, S. Muehlbrandt, D. Van Thourhout, B. Chen, R. Dinu, M. Sommer, C. Koos, M. Kohl, W. Freude, and J. Leuthold, Nat. Photonics **8**, 229 (2014).
[4] Z. Li, S. Zhang, N. J. Halas, P. Nordlander, and H. Xu, Small **7**, 593 (2011).
[5] M. Ayata, Y. Fedoryshyn, W. Heni, B. Baeuerle, A. Josten, M. Zahner, U. Koch, Y. Salamin, C. Hoessbacher, C. Haffner, D. L. Elder, L. R. Dalton, and J. Leuthold, Science **358**, 630 (2017).
[6] A. Akbari, R. N. Tait, and P. Berini, Opt. Express **18**, 8505 (2010).
[7] B. Desiatov, I. Goykhman, N. Mazurski, J. Shappir, J. B. Khurgin, and U. Levy, Optica **2**, 335 (2015).
[8] I. Goykhman, B. Desiatov, J. Khurgin, J. Shappir, and U. Levy, Nano Lett. **11**, 2219 (2011).
[9] A. Sobhani, M. W. Knight, Y. Wang, B. Zheng, N. S. King, L. V. Brown, Z. Fang, P. Nordlander, and N. J. Halas, Nat. Commun. **4**, 1643 (2013).
[10] B. Y. Zheng, Y. Wang, P. Nordlander, and N. J. Halas, Adv. Mater. **26**, 6318 (2014).
[11] M. Grajower, B. Desiatov, N. Mazurski, J. Shappir, J. B. Khurgin, and U. Levy, ACS Photonics **4**, 1015 (2017).
[12] I. Goykhman, B. Desiatov, J. Khurgin, J. Shappir, and U. Levy, Opt. Express **20**, 28594 (2012).
[13] J. J. Burke, G. Stegeman, and T. Tamir, Phys. Rev. B **33**, 5186 (1986).
[14] P. Berini, Opt. Express **7**, 329 (2000).
[15] F. Yang, J. R. Sambles, and G. W. Bradberry, Phys. Rev. B **44**, 5855 (1991).
[16] G. Veronis and S. Fan, J. Lightwave Technol. **25**, 2511 (2007).
[17] L. Liu, Z. Han, and S. He, Opt. Express **13**, 6645 (2005).
[18] W. Wang, Q. Yang, F. Fan, H. Xu, and Z. L. Wang, Nano Lett. **11**, 1603 (2011).
[19] H. W. Lee, M. A. Schmidt, R. F. Russell, N. Y. Joly, H. K. Tyagi, P. Uebel, and P. S. J. Russell, Opt. Express **19**, 12180 (2011).
[20] O. Lotan, C. L. C. Smith, J. Bar-David, N. A. Mortensen, A. Kristensen, and U. Levy, ACS Photonics **3**, 2150 (2016).
[21] C. L. C. Smith, B. Desiatov, I. Goykmann, I. Fernandez-Cuesta, U. Levy, and A. Kristensen, Opt. Express **20**, 5696 (2012).
[22] H.-H. Cheng, S.-W. Chen, Y.-Y. Chang, J.-Y. Chu, D.-Z. Lin, Y.-P. Chen, and J.-H. Li, Opt. Express **19**, 22125 (2011).
[23] V. A. Zenin, V. S. Volkov, Z. Han, S. I. Bozhevolnyi, E. Devaux, and T. W. Ebbesen, J. Opt. Soc. Am. B **28**, 1596 (2011).
[24] A. Boltasseva, T. Nikolajsen, K. Leosson, K. Kjaer, M. S. Larsen, and S. I. Bozhevolnyi, J. Lightwave Technol. **23**, 413 (2005).
[25] D. P. Waveguides, X. Shi, X. Zhang, Z. Han, U. Levy, and S. I. Bozhevolnyi, J. Lightwave Technol. **31**, 3361 (2013).
[26] Y. Chen, V. A. Zenin, K. Leosson, X. Shi, M. G. Nielsen, and S. I. Bozhevolnyi, Opt. Express **23**, 9100 (2015).
[27] J. Gosciniak, T. Holmgaard, and S. I. Bozhevolnyi, J. Lightwave Technol. **29**, 1473 (2011).
[28] T. Holmgaard, Z. Chen, S. I. Bozhevolnyi, L. Markey, A. Dereux, A. V. Krasavin, and A. V. Zayats, Opt. Express **16**, 13585 (2008).
[29] R. Zektzer, B. Desiatov, N. Mazurski, S. I. Bozhevolnyi, and U. Levy, Opt. Express **22**, 22009 (2014).
[30] S. Rao, F. G. Della Corte, and C. Summonte, J. Eur. Opt. Soc.: Publ. **5**, 10002 (2010).
[31] Y. Bian and Q. Gong, J. Opt. **16**, 15001 (2014).
[32] M.-S. Kwon, Opt. Express **19**, 8379 (2011).
[33] S. Zhu, T. Y. Liow, G. Q. Lo, and D. L. Kwong, Opt. Express **19**, 8888 (2011).
[34] V. Giannini, Y. Zhang, M. Forcales, and J. G. Rivas, Opt. Express **16**, 19674 (2008).
[35] Y. Bian and Q. Gong, Opt. Express **21**, 23907 (2013).
[36] C.-C. Huang, Opt. Express **440**, 2333 (2013).
[37] L. Chen, T. Zhang, X. Li, and W. Huang, Opt. Express **20**, 20535 (2012).
[38] D. Dai and S. He, Opt. Express **17**, 16646 (2009).
[39] Z. Zhu and T. Brown, Opt. Express **10**, 853 (2002).
[40] S. K. Selvaraja, E. Sleeckx, M. Schaekers, W. Bogaerts, D. Van Thourhout, P. Dumon, and R. Baets, Opt. Commun. **282**, 1767 (2009).